Chapter II

Materials and Experimental Techniques

This chapter deals with the basic information of the materials that are used in the present investigations. The theoretical details of the various techniques used for the preparation and characterization of polymeric materials are described.

2.1 Materials Employed in Preparing Polymer Nanocomposites

In the present study, all chemicals used were AR Grade.

2.1.1 Host Polymer

(i) Polystyrene

Molecular formula: [-C_8H_8-]

Chemical structure:

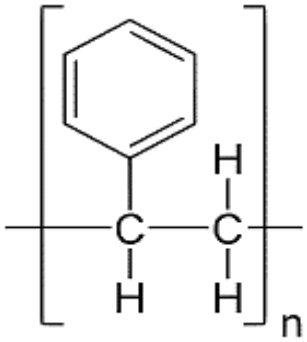

Molecular Weight : 100,000 – 400, 000 g/mol

Density : 0.96 – 1.05 gm/cm^3

Melting temperature: 260°C

Purchased from : National Chemicals

(ii) Polyvinyl Alcohol :

Molecular formula: [-C_2H_4O-]

Chemical structure:

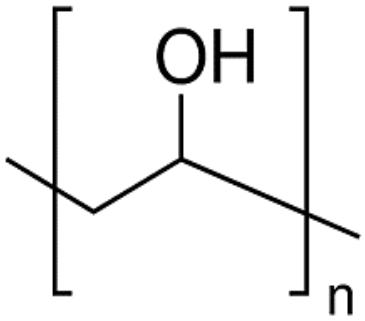

Molecular Weight : 85,000 – 124, 000 g/mol

Density : 1.19 – 1.31 gm/cm^3

Melting temperature: 228°C

Purchased from : Sigma Aldrich

2.1.2 Filler

(i) Aluminum oxide (Al_2O_3) :

Particle size: < 50 nm

Purchased from: Sigma Aldrich

(ii) Europium oxide (Eu_2O_3) :

Particle size: 30-50 nm

Purchased from: Alfa Aesar

(ii) Silicon dioxide (SiO_2) :

Particle size: 10-20 nm

Purchased from: Alfa Aesar

2.1.3 Salt

(i) Phosphoric Acid (H_3PO_4):

State: powder

Purchased from: Sigma Aldrich

2.1.4 Solvent

Toluene and deionized water were used as a solvent to dissolve polystyrene and PVA, respectively.

2.2 Sample Preparation Method

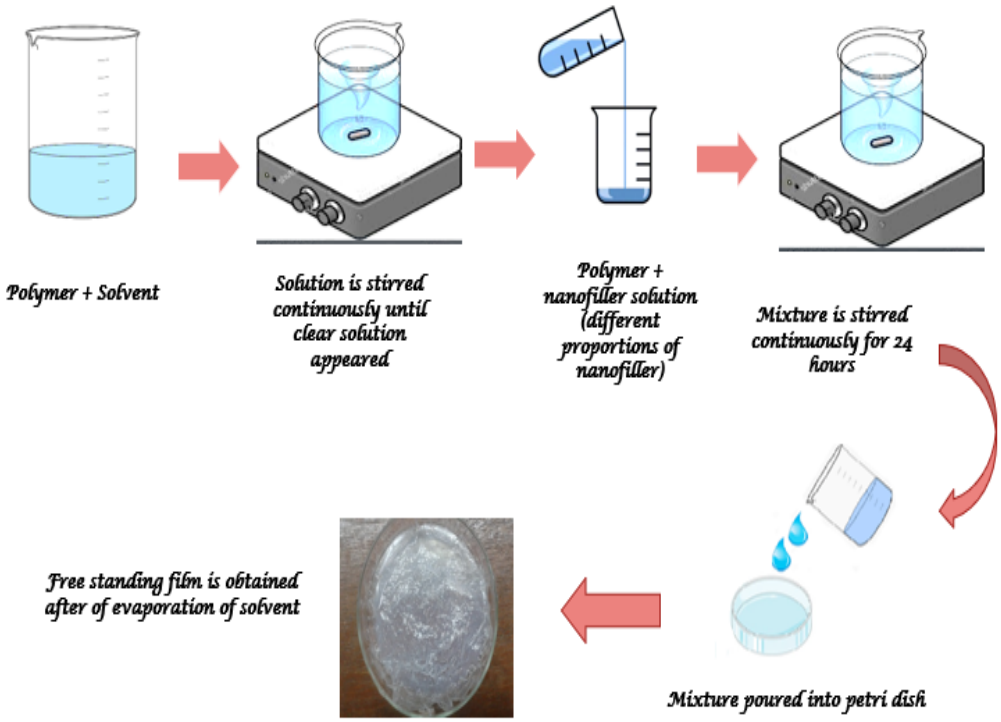

Figure 2.1 Schematic diagram of the sample preparation method.

The solution casting method was used to synthesize the samples (figure 2.1). Initially, the appropriate amount of polymer and nanoparticles was dissolved in the beaker using a solvent with constant stirring. The polymer solution was continuously stirred until a clear solution appeared. After the dissolution of the polymer, the solution of filler was added to the polymer solution. The mixture of polymer and filler was sonicated to achieve uniform dispersion of filler. This mixture was stirred for 24 hours for thorough interaction of polymer and filler. Lastly, The solution was poured into a Teflon petri dish, and the solvent was evaporated by placing it in an oven at 35˚C. After evaporation of the solvent, the free-standing film was peeled off and placed in a vacuum desiccator.

As the above-stated method, the following samples were prepared. Microanalytical balance was used to weigh the desired amounts of starting materials.

1. First Series: Polystyrene/Al_2O_3 Polymer Nanocomposites (PSA)

The amount of polystyrene and Al_2O_3 nanoparticles is varied in this series, namely, (1-x) wt% and x wt% (where x= 1, 2, 3, 4), respectively. Dopings of 1, 2, 3, and 4 wt% of Al_2O_3 nanoparticles in polystyrene are labeled as PA1, PA2, PA3, and PA4.

2. Second Series: Polystyrene/Eu_2O_3 Polymer Nanocomposites (PSE)

In the second series, the variation in the amount of polystyrene and Eu_2O_3 was similar to that of the first series. PSE1, PSE3, and PSE5 designate the composite films of 1, 3, and 5 wt% Eu_2O_3 doped polystyrenes.

3. Third Series: PVA/ H_3PO_4/SiO_2 Nanocomposite Polymer Electrolytes (PHS)

In the third series, PVA and H_3PO_4 (40 wt%) were fixed in composition, while SiO_2 was varied, *viz*., PHS2 (2 wt%), PHS4 (4 wt%), PHS6 (6 wt%), PHS8 (8 swt%), and PHS10 (10 wt%).

2.2.1 Thickness Measurement of Samples

The thickness of all samples was measured using a sensitive digital vernier caliper. PSA series and PSE thickness was about 120 µm, while the thickness of the PHS series was about 140 µm.

2.3 Irradiation Details

Swift heavy ion irradiation was carried out using the facility at IUAC, New Delhi. The facility uses a 15 UD Pelletron accelerator. The schematic

diagram of 15 UD Pelletron accelerator is shown in figure 2.2. All samples were irradiated in the beamline used for material irradiation, as shown 2.3. Figure 2.4 shows the irradiation chamber. The polymeric films were irradiated with a 90 MeV carbon ion beam at the fluences of 1 x 10^{11} and 1 x10^{12} ions cm^{-2}.

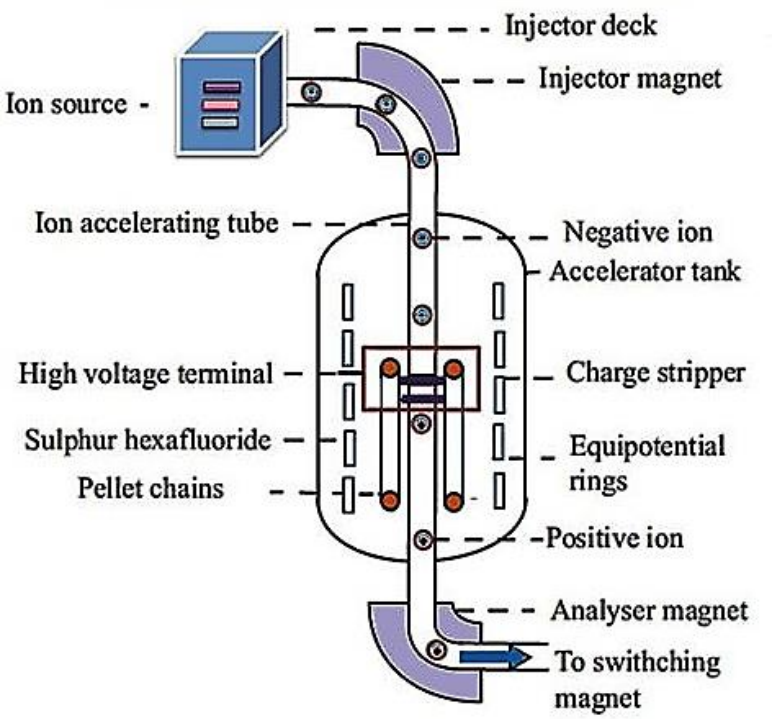

Figure 2.2 15 UD Pelletron accelerator at IUAC, New Delhi.

Figure 2.3 Beam line for material irradiation.

Figure 2.4 Irradiation chamber of Material science.

2.3.1 Pelletron Accelerator

The 15 UD Pelletron Accelerator, a Tandem Van De Graff type accelerator has been installed at Inter-University Accelerator Centre (IUAC), New Delhi for applied and basic research in atomic physics, materials science, and nuclear science. This accelerator is used to accelerate any ions from proton to uranium except inert gases. It is installed in a steel tank of height 26.57 m and diameter 5.5 m, having vertical geometry. The tank is filled with sulphur hexafluoride gas to thwart discharging and sparking (to obtain insulation). A Multi Cathode Source of Negative Ion by Cesium Sputtering (SNICS) acts as an ion source for negative ions, which are momentum analyzed by a dipole magnet, known as the injector magnet.

A voltage terminal of height 3.81 mm and width 1.52 mm at the center of the tank is charged to high potential in the range of 4 to 16 MV with the help of an electrostatic charge transfer device. This terminal is coupled with the tank vertically through ceramic-titanium diffusion-bonded accelerating tubes. These accelerating tubes help to maintain potential gradient. The negative ions accelerate toward the terminal, attaining an energy V MeV (V= terminal potential). The terminal contains an offset quadrupole lens, a Faraday cup, an

assembly of a foil stripper, and a gas stripper. When the negative ions are passed through this assembly of strippers, they strip off a few electrons and convert negative ions into positive ions. These positive ions get accelerated to high energy towards the bottom of the tank. Thus, the energy gain by the ions which come out from the accelerator column is given by

$$E = V_{\pi}\ (q + 1)\ \text{MeV} \ldots\ldots\ldots\ldots\ldots (2.1)$$

Where, V_{π} = terminal potential in MV, q = charge state after stripping

Therefore, a heavy ion's final kinetic energy having charge state q is (q+1) x 15 MeV. These high energetic ions need to be analyzed by a 90° bent analyzer magnet and finally sent to the desired beam-hall using a multiport switching magnet. The offset quadrupole lens and Faraday cup are used to choose an appropriate charge state after stripping.

2.3.2 Irradiation Procedure

The irradiation of samples is usually executed at the materials science beamline premise. This beamline is situated in such a way that it makes an angle of 15° with an unswitched direct beam and keeps at ultra-low pressure of about 10^{-9} torr. Targets are mounted on the sliding ladder, which is a specially designed copper block of a rectangular cross-section. A double tape is used to mount the polymeric films of size ~1.5 × 1.5 cm^2 on the sliding ladder. Figure 2.5 shows an image of irradiated polymeric films mounted on a sliding ladder. During irradiation, the ladder was placed at the right angle to the beamline in the target chamber. The irradiation was made in the area of 1 cm × 1 cm of the sample by scanning the beam in the X-Y plane. The ladder is placed in the high vacuum target chamber maintained at about 10^{-6} torr of pressure after inserting the target ladder. The target ladder's up and down movements are controlled by a stepper motor configured with a mechanical assembly. The beam is concentrated on the sample with the help of a magnetic quadrupole and a steerer. A quartz crystal is employed to check whether the ion beam is falling on it or not. It is mounted on four sides of the sliding ladder. The ion fluence is calculated from the current integrator and ladder current. However, the entire setup is computer controlled and is managed from the control room

The current was usually kept small at 0.5 pnA to prevent thermal decomposition of the polymer. The nuclear stopping power and electronic

stopping power due to 90 MeV carbon ion beam irradiation were calculated using SRIM.

Figure 2.5 Sample holder for SHI irradiation at IUAC, New Delhi.

2.3.3 Results obtained from SRIM

Sample	Projectile Range (µm)	Electronic Stopping Power (eV/Å)	Nuclear Stopping Power (eV/Å)
PA4	251.72	21.34	1.133×10^{-2}
PSE5	233.28	25.21	1.377×10^{-2}
PHS10	258.61	21.54	1.115×10^{-2}

Table 2.1 SRIM calculation for 90 MeV carbon ion irradiated polymeric films.

2.3.4 Gamma Radiation Chamber

The Gamma Chamber has been installed at IUAC, New Delhi. The radioactive isotope of Cobalt-60 is employed as a gamma radiation source and, its lifetime is about 5.27 years. Gamma chamber contains the radiation source, central drawer with sample chamber, driving system, biological shield, external cabinet and control panel. An image of the gamma chamber is shown in figure 2.6. The samples for irradiation are kept inside an irradiation chamber situated in

the vertical drawer. The control panel can adjust the motion of the vertical drawer. The polymer composites were also irradiated with 25 and 50 kGy doses of gamma rays. The dose rate was maintained at 3.7 kGy/hr.

Figure 2.6 Gamma chamber 1200 at IUAC, New Delhi.

2.3.5 Irradiation Time Calculation

(i) Ion Beam Irradiation

$$\text{Time} = \frac{\text{ion fluence x area of sample } (\text{cm}^2)}{\text{current (pnA)x } 6.25 \text{ x} 10^9} \ldots\ldots\ldots\ldots (2.2)$$

For example :

Ion fluence = 1 x 10^{12} ions/cm^2

Current = 0.5 pnA

Area of polymeric film = 1 x 1 cm^2

Then, the time for ion beam irradiation is equal to 32 seconds.

(ii) Gamma Radiation

$$\text{Time} = \frac{1}{\text{Dose rate}} \text{ x Required dose} \ldots\ldots\ldots\ldots\ldots\ldots\ldots\ldots (2.3)$$

For example :

Dose rate = 3.27 kGy/hr

The required dose = 50 kGy

Then, the time for gamma exposure comes to be 15 hr 17 min 4 sec.

2.4 Experimental Techniques

2.4.1 X-ray Diffraction (XRD)

X-ray Diffraction is a powerful technique to recognize crystalline phases existing in the samples. It is also used to determine the crystal structure as well as the grain size, strain and stress state, preferred orientation and phase composition, etc. [1,2]. X-ray diffraction is the phenomenon of superposition of X-ray scattered from atoms that are arranged periodically in the crystal. A schematic diagram of the reflection of X-ray from two parallel planes of atoms is shown in figure 2.7. The peaks of the X-ray diffraction pattern are achieved due to interference [3,4]. The interference is related to the atomic distribution and is correlated to the interplanar distance, d, through the following equation [5].

$$n\lambda = 2d\ sin\theta \ldots\ldots\ldots\ldots (2.4)$$

λ = wavelength of X-rays, n = order of reflection and θ = grazing angle of incidence

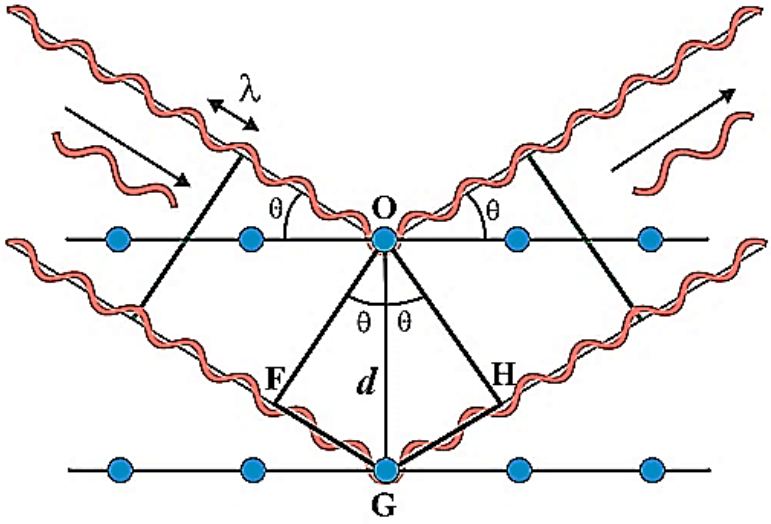

Figure 2.7 Reflection of X-rays from two parallel planes of atoms in a crystal.

The average crystallite size (D) of nanocomposites is determined by Scherrer's formula

$$D = \frac{K\lambda}{\beta \cos\theta} \ldots\ldots\ldots\ldots (2.5)$$

Where K (= 0.9) is the shape factor. λ (= 1.5416 Å) is the wavelength of X-ray; β is an FWHM of intense peaks.

Equipment used

The X-ray diffraction patterns of all polymeric films were obtained by Bruker D8 advance diffractometer available at IUC, Indore, as shown in figure 2.8. Cu-Kα source of wavelength 0.15406 nm was employed as the X-ray source. The Bragg angle Θ was varied as 2Θ = 10˚ to 60˚ with 1˚ sec^{-1} scan speed and 0.05˚ step width.

Figure 2.8 Bruker D8 advance x-ray diffractometer.

2.4.2 Fourier Transform Infrared (FT-IR) Spectroscopy

FTIR spectroscopy is an important technique for identifying functional groups in organic and inorganic materials [6,7]. In this, molecules are excited to higher energy vibrational levels through infrared absorption. When IR radiation passes through the material, part of it is absorbed by the material and the rest is transmitted through it. Therefore, the resulting spectra describe molecular absorption and transmission, producing a fingerprint of the material. Molecules absorb only specific frequencies of radiation that match with their natural frequencies of vibration. This increases the amplitude of vibration of bonds [8]. Alteration of vibrational and rotational states of molecules produces the absorption in the infrared region. The intensity of absorption is influenced by the effectiveness of the transfer of infrared photon energy to the molecules. Additionally, the size of the peaks indicates the amount of sample. No two

identical molecular structures have the same IR spectra. The interferometer is used to obtain an interferogram of the sample, which is obtained by the Fourier transform of the interferogram [9,10].

Equipment used

JASCO – 4600 Fourier Transform Infra-Red spectrometer was used to record FTIR spectra of all samples. The spectra of PS base nanocomposites were recorded in Transmittance mode in the range of 400-4000 cm^{-1}, whereas the spectra of PVA-based nanocomposite polymer electrolytes were recorded in Attenuated total reflection mode in the range of 650-4000 cm^{-1}. The spectrometer is illustrated in figure 2.9.

Figure 2.9 JASCO – 4600 Fourier Transform Infra-Red spectrometer.

2.4.3 Ultraviolet-Visible (UV-VIS) Spectroscopy

Ultraviolet-visible spectroscopy yields attenuation of a beam of light (UV/visible) as it traverses through the material sample or is reflected from its surface. The amount of absorbed energy depends on the compound's structure, sample thickness, and radiation wavelength. In this case, the radiation interaction involves the excitation of electrons from the ground state, followed by de-excitation. The absorbance data is useful to determine the energy band gap of compound and impurity levels inside a compound. The light absorption by the material is directly proportional to the path length (L) and concentration of absorbing species (c), as prescribed by the Beer-Lambert law [11]:

$$A = log_{10}\left(\frac{I_0}{I}\right) = \varepsilon\, c\, L \ \ldots\ldots\ldots\ldots (2.6)$$

where I_0 and I are the intensity of incident and transmitted light at a given wavelength, respectively. ε is the molar absorption coefficient. Beer-Lambert law provides information about the molar absorption coefficient and wavelength at maximum absorption, often helpful in identifying the compound. The absorption coefficient (α) is calculated from absorption (A) and thickness of the sample (d) using the following equation:

$$\alpha = \frac{A}{d} \ldots\ldots\ldots\ldots\ldots\ldots\ldots\ldots\ldots\ldots\ldots\ldots (2.7)$$

Due to the incorporation of filler, the absorption edge is found to shift towards a shorter or longer wavelength. This shift is related to the optical band gap through Tauc's equation as follows [12]:

$$(\alpha hv)^n = B\ (hv - E_g) \ldots\ldots\ldots\ldots (2.8)$$

where n is a parameter with values of 0.5 or 2 represents indirect allowed or direct allowed transition across the bandgap while B is a constant. The optical bandgap is procured by extrapolating the high energy side absorption curve giving as bandgap the intercept on the X-axis of the graph of $(\alpha hv)^n$ against *hv*.

The number of C_6 rings in the compact carbonaceous cluster (M) is given by the following relation [13]:

$$E_g = 2\,|\beta|\,M^{-0.5} \ldots\ldots\ldots\ldots\ldots\ldots (2.9)$$

$|\beta|$ = Bond integral

However, The number of carbon atoms per conjugation length (N) can be determined by the following formula [14]:

$$E_g = \frac{34.3}{\sqrt{N}} \ldots\ldots\ldots\ldots\ldots\ldots\ldots\ldots (2.10)$$

Equipment used

All samples' absorption spectra were recorded using Jasco V-730 spectrophotometer in the range of 200- 800 nm. The instrument is depicted in figure 2.10. This facility was available in the Department of Chemistry. Pristine and irradiated polymeric films were mounted in 1 x 1 cm^2 window area of the sample holder.

Figure 2.10 JASCO V-730 spectrophotometer.

2.4.4 Photoluminescence Spectroscopy

Photoluminescence is the spontaneous emission of light by the sample upon absorbing UV, visible or infrared radiation. After absorption of energy, the outermost orbital electrons of atoms and molecules excite from ground level to excitation level [15]. The luminescence process is classified into two classes, namely, phosphorescence and fluorescence. Usually, in the fluorescence process, the emission of light takes place within a nanosecond, whereas, in the phosphorescence process, it takes from microsecond to hours or days [16] for emission to take place. The luminescence material is the material that can emit light as a result of the absorption of excitation energy. These materials are often known as phosphors. They consist of a very small amount of impurity because, at the high amount of impurity, the output of photoluminescence decreases [17–19].
In the luminescence process, the incident energy is absorbed by host material or doped impurities. Most of the time, the incident energy is absorbed by impurity, which then excites a higher energy level. Such impurity is known as an activator. The activator is returned to the ground state by the emission of visible radiation [20]. If the activator is not efficient for excitation energy absorption, another type of impurity known as a sensitizer may come into play. It can transfer the absorbed energy to the activator [18,21].

Equipment used

Shimadzu RF-5301 spectrofluorophotometer was used to record photoluminescence spectra of all samples. The instrument uses 150 W xenon lamp radiation as the excitation source. This facility is available at the Department of Applied Science, Faculty of Technology, M. S. University of Baroda, Vadodara. The spectrofluorophotometer is depicted in figure 2.11.

Figure 2.11 Shimadzu RF-5301 spectrofluorophotometer.

2.4.5 Thermoluminescence

Thermoluminescence refers to the process of emission of light from an insulator or a semiconductor after the absorption of energy from ionizing radiation [19,22]. This absorbed energy excites free electrons and free holes, followed by trapping these electrons and holes in defects or trapping sites within the energy gap. The emission of light takes place when the sample is heated at a constant rate. In the case of a polymer, the trapped charges can be freed through macromolecules' motion during heating. These freed electrons recombine through light emission. Hence, TL maxima can be noticed. These maxima are related to the polystyrene chain's different molecular relaxation mechanisms, such as γ-, δ- and β- relaxation [23]. In the case of polymers, the forms of traps are unlike those in a crystalline material, such as irregularly shaped voids, molecules, and free radicals [24]. The origin of thermoluminescence (TL) maxima in polymers was first proposed by Pannel and Manning [25]. The TL glow curve of a polymer consists of a broad peak. Few reports on TL study of pure and doped polymers are available [23–26]. Applications of thermoluminescence are found in the areas of Health Physics and biomedical sciences such as personal dosimetry, retrospective,

and environmental dosimetry, diagnostic radiology, and radiotherapy dosimetry. Thermoluminescence is also useful in solid-state iconography, space, and environmental monitoring [27–29]. Several theoretical approaches are made to estimate TL parameters like frequency factor and activation energy, which help understand charge transfer processes. TL glow curve of a polymer normally comprises of overlapping of many peaks. Hence the glow curve deconvolution method is more appropriate for the analysis than other methods for polymers.

Glow Curve Deconvolution Method:

The TL glow curves of polymer composites were analyzed using the glow curve deconvolution method. In this method, the curve is segregated into several distinct peaks [30]. This method was established by Kitis et al. and is employed for first-order kinetics, second-order kinetics, and general order kinetics [31].

First-order kinetics equation

$$I(T) = I_m \exp(1 + \frac{E_a}{k_B T}\left(\frac{T-T_m}{T_m}\right) - \frac{T^2}{{T_m}^2}\left(1 - \frac{2k_B T}{E_a}\right)\exp\left(\frac{E_a}{k_B T}\left(\frac{T-T_m}{T_m}\right)\right) - \frac{2k_B T_m}{E_a} \quad \ldots\ldots\ldots\ldots\ldots\ldots\ldots\ldots\ldots\ldots\ldots\ldots\ldots\ldots\ldots\ldots\ldots\ldots (2.11)$$

Equation of the frequency factor for First-order kinetics

$$s = \frac{\beta E_a}{k_B T_m^2}\exp\left(\frac{E_a}{k_B T}\right) \ldots\ldots\ldots\ldots\ldots\ldots\ldots\ldots (2.12)$$

Second-order kinetics equation

$$I(T) = 4I_m \exp\left(\frac{E_a}{k_B T}\left(\frac{T-T_m}{T_m}\right)\right)[\frac{T^2}{{T_m}^2}\left(1 - \frac{2k_B T}{E_a}\right)\exp\left(\frac{E_a}{k_B T}\left(\frac{T-T_m}{T_m}\right)\right) + 1 - \frac{2k_B T_m}{E_a}]^{-2} \ldots\ldots\ldots\ldots\ldots\ldots\ldots\ldots\ldots\ldots\ldots\ldots\ldots\ldots\ldots\ldots\ldots\ldots (2.13)$$

Equation of the frequency factor for second-order kinetics

$$s = \frac{\beta E_a}{k_B T_m^2\,(1 + \frac{2k_B T_m}{E_a})}\exp\left(\frac{E_a}{k_B T_m}\right) \ldots\ldots (2.14)$$

General order kinetics equation

$$I(T) = I_m b^{b-1}\exp\left(\frac{E_a}{k_B T}\left(\frac{T-T_m}{T_m}\right)\right)[(b-1)\frac{T^2}{{T_m}^2}\left(1 - \frac{2k_B T}{E_a}\right)\exp\left(\frac{E_a}{k_B T}\left(\frac{T-T_m}{T_m}\right)\right) + 1 + (b-1)\frac{2k_B T_m}{E_a}]^{(b-1)} \ldots\ldots\ldots\ldots (2.15)$$

Equation of the frequency factor for general order kinetics is,

$$s = \frac{\beta E_a}{k_B T_m^2\,[1+\frac{2k_B T_m (b-1)}{E_a}]}\exp(\frac{E_a}{k_B T_m}) \ldots (2.16)$$

where, T and T_m are TL temperature and temperature at maximum intensity (I_m), respectively. E_a, $k_{B,}$ and β are activation energy, Boltzmann's constant and heating rate, respectively.

Equipment used

TL measurement of all samples was carried out using Thermofisher – Harshaw TLD reader (Model HT 3500) with a heating rate of 3 K/s at IUAC, New Delhi. Figure 2.12 shows the TL instrument (Thermofisher – Harshaw TLD reader - Model HT 3500).

Figure 2.12 Thermofisher – Harshaw TLD reader (Model HT 3500).

2.4.6 Impedance Spectroscopy

Impedance spectroscopy is an essential tool to study electrical responses such as bulk conductivity and transport processes. The response of material through impedance spectroscopy correlates with a parallel combination of resistor and capacitor, as depicted in figure 2.13.

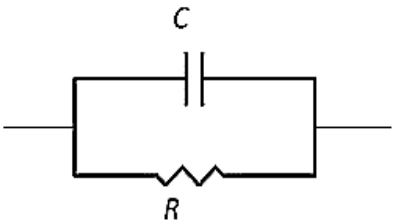

Figure 2.13 A parallel combination of capacitance and resistance.

Real and imaginary parts of the impedance are determined from bulk resistance (R) and bulk capacitance (C) using the equations:

$$Z' = \frac{R}{1+(\omega RC)^2} \ldots\ldots\ldots\ldots (2.17)$$

$$Z'' = \frac{\omega R^2 C}{1+(\omega RC)^2} \ldots\ldots\ldots\ldots (2.18)$$

The plot of Z'' versus Z' is known as the Nyquist plot, as depicted in figure 2.14. The plot contains a depressed semicircle in the high-frequency region followed by a spike in the low-frequency region. The intercept on the real part axis gives the value of bulk resistance.

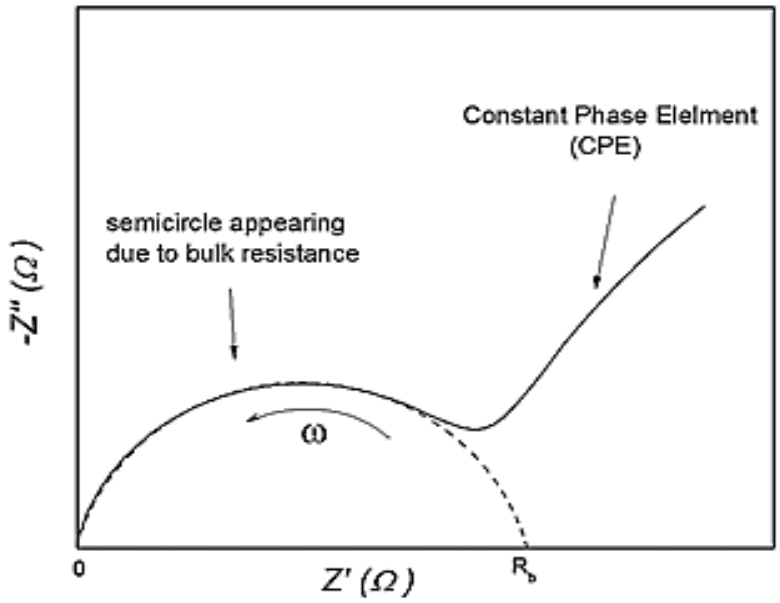

Figure 2.14 Nyquist plot.

The ionic conductivity of the sample is determined by the value of bulk resistance R_b using the following equation :

$$\sigma = \frac{t}{R_b A} \ldots\ldots\ldots\ldots\ldots\ldots (2.19)$$

2.4.6.1 Frequency-dependent A.C. Conductivity

Often, it is expressed in terms of Siemens/meter. In the case of polymers, although free electrons are present but are not connected to the macromolecular chain structure. However, thermoplastic polymers such as PMMA, PS, etc. have very low amounts of free electrons, indicating thermoplastic polymers' low conductivity. Ohm's law states that the conductivity is the ratio of current density (J) and electric field (E):

$$\sigma = \frac{J}{E} \ldots\ldots\ldots\ldots\ldots\ldots\ldots\ldots\ldots\ldots\ldots\ldots (2.20)$$

In the case of a capacitor, the electric field intensity derives from the potential difference, V, between the parallel plates and thickness, t, of the sample as follows:

$$E = \frac{V}{t} \ldots\ldots\ldots\ldots\ldots\ldots\ldots\ldots\ldots\ldots\ldots\ldots\ldots\ldots (2.21)$$

Since $J = \frac{\varepsilon}{t}\frac{dV}{dt} = \frac{\varepsilon}{t} Vj\omega$

So,

$$\sigma = \frac{J}{E} = \varepsilon j\omega = (\varepsilon' - j\varepsilon'')j\omega \ldots\ldots\ldots (2.22)$$

A.C. conductivity is the real part

So, $$\sigma = \varepsilon''\omega \ldots\ldots\ldots\ldots (2.23)$$

2.4.6.2 Jonscher's Power Law

Several theories account for the dispersion behavior of solid polymer electrolytes. In all, Jonscher's power law successfully describes ion transport properties as follows:

$$\sigma(\omega) = \sigma_{dc} + A\omega^n \ldots\ldots\ldots\ldots\ldots\ldots\ldots (2.24)$$

σ(ω) = conductivity at a particular frequency, σ_{dc} = DC conductivity, n = exponent and having a value between 0 and 1, A=constant. Equation 2.23 is often known as a power law of a. c. behavior.

2.4.6.3 Dielectric Response

J. C. Maxwell was the first to discover dielectric material. Later it was pursued by Debye. The dielectric permittivity of a material depends on the material form's orientation, frequency of the signal applied, pressure, and the material's molecular structure and temperature. The following equation determines the complex permittivity:

$$\varepsilon^* = \varepsilon' - \varepsilon'' \ldots\ldots\ldots\ldots\ldots\ldots\ldots\ldots\ldots\ldots\ldots (2.25)$$

where ε' and ε" are dielectric constant and dielectric loss, respectively. The dielectric loss is defined as energy loss during A.C. operation and is independent of the geometry of the capacitor. The structure of a dielectric material consists of a charge distribution that is polarizable under the influence of an externally applied electric field and results in a high degree of charge formation. These charges are stored on the capacitor plates. The dielectric constant is defined as:

$$\varepsilon' = \frac{C_p}{C_0} \ldots\ldots\ldots\ldots\ldots\ldots\ldots\ldots\ldots\ldots\ldots (2.26)$$

where $C_0 = \frac{\epsilon_0 A}{t}$, the value of the vacuum's permittivity, considered as 8.85 x 10^{-12} F/m, t, and A are the thickness of the sample and area of electrodes, respectively.

Equipment used

LCR meter (Agilent – 16452A) at Department of Physics, Gujarat University was used to study the electrical properties of PS/Eu_2O_3 and PVA/H_3PO_4/SiO_2 samples, as shown in figure 2.15. Whereas, electrical properties of other samples were measured using Solatron Impedance Analyser available in the department of The M. S. University of Baroda. The measurement was carried out in the frequency range of 100 Hz to 1 x 10^6 Hz.

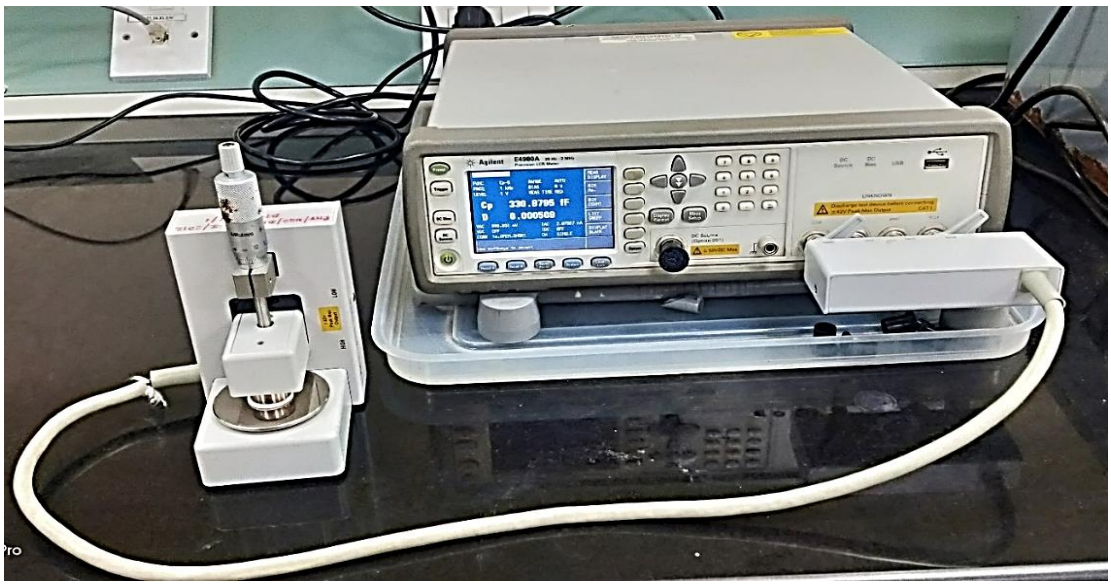

Figure 2.15 LCR meter (Agilent – 16452A).

2.4.7 Differential Scanning Calorimetry (DSC)

Thermal analysis of polymers is usually carried out using different techniques such as differential thermal analysis, differential scanning calorimetry (DSC), and dynamic mechanical, thermal analysis. These methods are employed to study the physical and chemical properties of the material. DSC is used here to explore the thermo-physical properties of polymers. In this method, the thermal properties of the sample are studied with respect to a reference sample. The reference may be an empty aluminum pan or an aluminum pan with inert material. The prepared sample and the reference are maintained at nearly identical temperatures throughout the experiment. Different amounts of heat required to raise the sample's temperature and the reference are studied as functions of

temperature. The underlying phenomenon is that different heat amounts are required to maintain the sample at the same temperature as that of the reference when the sample experiences phase transition. Different amounts of heat flow through the sample, depending upon the process being either exothermic or endothermic. Glass transition temperature is the temperature below which polymers become hard or glassy. Above T_g, the polymer becomes rubbery. DSC is thus used to determine the polymer's glass transition temperature, melting temperature, and crystallinity [32,33]. The following equation defines the crystallinity of the polymer [34]:

$$X_c = \frac{\Delta H_m}{\Delta H_{m,0}} \quad \ldots\ldots\ldots\ldots\ldots\ldots\ldots\ldots\ldots\ldots (2.27)$$

where, ΔH_m and $\Delta H_{m,0}$ are melting enthalpy per gram of the material and melting enthalpy per gram of the 100% crystalline material.

Equipment used

Differential scanning calorimeter SII EXSTAR 6000, DSC 6220 was used to study polymers' thermal property and is depicted in figure 2.16. The calorimetry was performed on a 2 mg sample under an environment of nitrogen gas with its flow rate of 60 ml/min. During this experiment, the heating rate was maintained at 10˚/min.

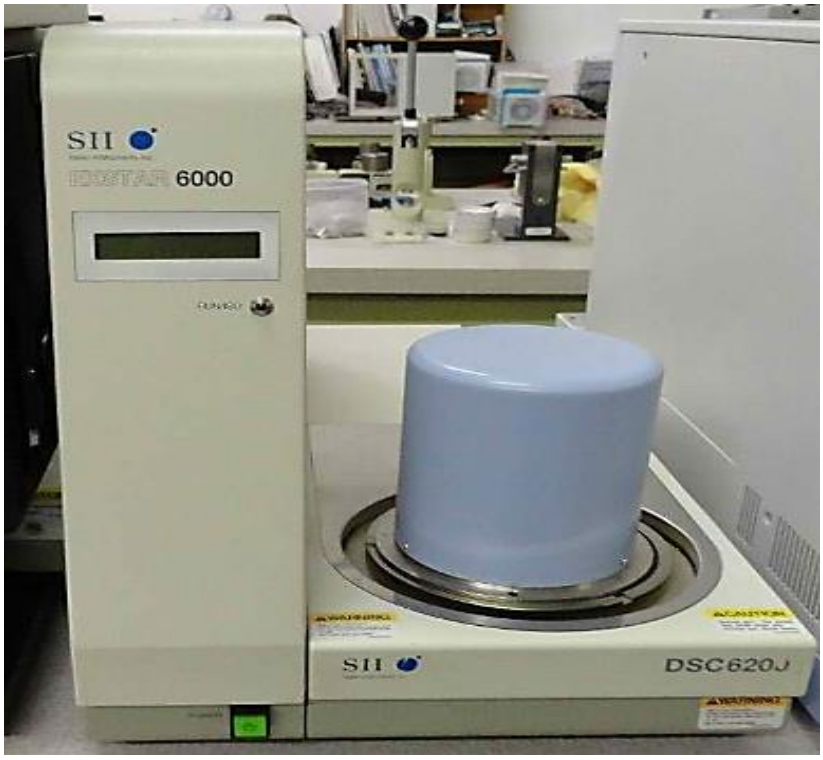

Figure 2.16 Differential scanning calorimetry (SII EXSTAR 6000, DSC 6220).

2.4.8 Atomic Force Microscopy

Atomic force microscopy is one of the crucial scanning probe microscopes that gives the high resolution of a nanometer's order. The AFM contains a cantilever with a sharp tip, used for scanning the specimen. This pointed tip is made up of either silicon or Si_3N_4 and is used to examine material. When the sharp tip is brought closer to the sample, van der Waal's force between the tip and the sample surface appears. This force causes a deflection of the cantilever, helping to detect the laser spot's reflection from the top of the cantilever.

However, the laser deflection system is bulky and costly. Therefore, the piezoresistive AFM probe was used in place of the laser deflection system. Usually, a piezoelectric tube is used to mount the sample and shift the sample in the x-y direction to the scan sample. Z-direction is maintained in such a way that the force remains constant. Moreover, AFM operates in three modes, namely contact mode, non-contact mode, and dynamic contact mode. In the present case, the tapping mode is used to determine the surface roughness of pristine and the irradiated polymer.

Figure 2.17 AFM set up at IUAC, New Delhi.

Equipment used

The roughness of PVA/H_3PO_4/SiO_2 nanocomposite polymer electrolytes was measured using AFM Nanoscope digital instrument, Canberra, USA. Figure 2.17 shows AFM setup at IUAC, New Delhi. The roughness of PS/Al_2O_3 and PS/Eu_2O_3 was determined using Nanoscope-E, a Digital instrument from the USA at IUC, Indore.

References:

[1] A. A. Bunaciu, E. gabriela Udriştioiu, H. Y. Aboul-Enein, X-Ray Diffraction: Instrumentation and Applications, Crit. Rev. Anal. Chem. 45 (2015) 289–299. https://doi.org/10.1080/10408347.2014.949616.

[2] P. Bindu, S. Thomas, Estimation of lattice strain in ZnO nanoparticles: X-ray peak profile analysis, J. Theor. Appl. Phys. 8 (2014) 123–134. https://doi.org/10.1007/s40094-014-0141-9.

[3] B. Fultz, J. Howe, Transmission Electron Microscopy and Diffractometry of Materials, Springer Berlin Heidelberg, Berlin, Heidelberg, 2008. https://doi.org/10.1007/978-3-540-73886-2.

[4] L. E. A. Harold, P. Klug, X-ray diffraction procedures : for polycrystalline and amorphous materials, 2nd editio, Wiley-VCH Verlag, 1974.

[5] W. L. Bragg, The Diffraction of Short Electromagnetic Waves by a Crystal, Proc. Camb. Philol. Soc. 17 (1913) 43–57.

[6] A. Elena, I. Gozescu, A. Dabici, P. Sfirloaga, Z. Szabadai, Organic Compounds FT-IR Spectroscopy, in: Macro To Nano Spectrosc., InTech, 2012. https://doi.org/10.5772/50183.

[7] J. Coates, Interpretation of Infrared Spectra, A Practical Approach, John Wiley & Sons, Ltd, Chichester, UK, 2006. https://doi.org/10.1002/9780470027318.a5606.

[8] S. W. B. P. Straughan, Spectroscopy Volume 2, John Wiley & Sons, Ltd, 1976.

[9] J. A. D. H. Peter R. Griffiths, Fourier Transform Infrared Spectrometry. vol.171, John Wiley & Sons, Ltd, 2007.

[10] O. Faix, Fourier Transform Infrared Spectroscopy, in: 1992: pp. 83–109. https://doi.org/10.1007/978-3-642-74065-7_7.

[11] S. R. C. Douglas A skoog, Donald M. West, F. James Holler, Fundamentals of Analytical chemistry, 8th ed., 2003.

[12] J. Tauc, R. Grigorovici, A. Vancu, Optical Properties and Electronic Structure of Amorphous Germanium, Phys. Status Solidi. 15 (1966) 627–637. https://doi.org/10.1002/pssb.19660150224.

[13] J. Robertson, E. P. O'Reilly, Electronic and atomic structure of amorphous carbon, Phys. Rev. B. 35 (1987) 2946–2957.

https://doi.org/10.1103/PhysRevB.35.2946.

[14] D. Fink, W. H. Chung, R. Klett, A. Schmoldt, J. Cardoso, R. Montiel, M. H. Vazquez, L. Wang, F. Hosoi, H. Omichi, P. Goppelt-Langer, Carbonaceous clusters in irradiated polymers as revealed by UV-Vis spectrometry, Radiat. Eff. Defects Solids. 133 (1995) 193–208. https://doi.org/10.1080/10420159508223990.

[15] J. W. Lichtman, J. A. Conchello, Fluorescence microscopy, Nat. Methods. 2 (2005) 910–919. https://doi.org/10.1038/nmeth817.

[16] S. Svanberg, Atomic and Molecular Spectroscopy, Springer Berlin Heidelberg, Berlin, Heidelberg, 2004. https://doi.org/10.1007/978-3-642-18520-5.

[17] E. Danielson, J. H. Golden, E. W. McFarland, C. M. Reaves, W. H. Weinberg, X. Di Wu, A combinatorial approach to the discovery and optimization of luminescent materials, Nature. 389 (1997) 944–948. https://doi.org/10.1038/40099.

[18] C. R. Ronda, Luminescence, Wiley, 2007. https://doi.org/10.1002/9783527621064.

[19] G. Blasse, B. C. Grabmaier, Luminescent Materials, Springer Berlin Heidelberg, Berlin, Heidelberg, 1994. https://doi.org/10.1007/978-3-642-79017-1.

[20] K. N. Shinde, S. J. Dhoble, H. C. Swart, K. Park, Phosphate Phosphors for Solid-State Lighting, Springer Berlin Heidelberg, Berlin, Heidelberg, 2012. https://doi.org/10.1007/978-3-642-34312-4.

[21] G. Blasse, Chapter 34 Chemistry and physics of R-activated phosphors, in: 1979: pp. 237–274. https://doi.org/10.1016/S0168-1273(79)04007-1.

[22] R. Chen, Glow Curves with General Order Kinetics, J. Electrochem. Soc. 116 (1969) 1254. https://doi.org/10.1149/1.2412291.

[23] E. Dobruchowska, L. Okrasa, I. Glowacki, J. Ulanski, G. Boiteux, The ‘wet dog’ effect in polymers as seen by thermoluminescence, Polymer 45 (2004) 6027–6035. https://doi.org/10.1016/j.polymer.2004.06.019.

[24] L. F. Pender, R. J. Fleming, Thermoluminescence in polystyrene, J. Phys. C Solid State Phys. 10 (1977) 1571–1586. https://doi.org/10.1088/0022-3719/10/9/027.

[25] J. H. Pannell, B. Manning, Production of a Blue Color in Irradiated Plastic

Scintillators, J. Chem. Phys. 23 (1955) 1368–1369. https://doi.org/10.1063/1.1742304.

[26] A. Ortiz-Morales, J. Ortiz-Lopez, E. Cruz-Zaragoza, R. Gómez-Aguilar, Appl. Radiat. Isot. 102 (2015) 55–62. https://doi.org/10.1016/j.apradiso.2015.04.013.

[27] M. J. Aitken, Thermoluminescence dating, Academic Press, London, n.d.

[28] A. K. Singhvi, Y. P. Sharma, D. P. Agrawal, Thermoluminescence dating of sand dunes in Rajasthan, India, Nature. 295 (1982) 313–315. https://doi.org/10.1038/295313a0.

[29] T. Niewiadomski, J. Koperski, E. Ryba, Natural Radiation in Poland and Its Disturbance in An Urban Environment, Health Phys. 38 (1980) 25–32. https://doi.org/10.1097/00004032-198001000-00004.

[30] G. Kitis, J. M. Gomez-Ros, J. W. N. Tuyn, Thermoluminescence glow-curve deconvolution functions for first, second and general orders of kinetics, J. Phys. D. Appl. Phys. 31 (1998) 2636-2641. https://doi.org/10.1088/0022-3727/31/19/037.

[31] G. Kitis, J. M. Gomez-Ros, Thermoluminescence glow-curve deconvolution functions for mixed order of kinetics and continuous trap distribution, Nucl. Instruments Methods Phys. Res. Sect. A Accel. Spectrometers, Detect. Assoc. Equip. 440 (2000) 224–231. https://doi.org/10.1016/S0168-9002(99)00876-1.

[32] P. J. Haines, Thermal Methods of Analysis, Springer Netherlands, Dordrecht, 1995. https://doi.org/10.1007/978-94-011-1324-3.

[33] Stevens Malcolm, Polymer Chemistry, Oxford University Press, 1999.

[34] G. B. Patel, S. Bhavsar, N. L. Singh, F. Singh, P. K. Kulriya, SHI induced modification in structural, optical, dielectric and thermal properties of poly ethylene oxide films, Nucl. Instruments Methods Phys. Res. Sect. B 379 (2016) 156-161. https://doi.org/10.1016/j.nimb.2016.04.018.